Operation of Flying Capacitor Multilevel Converters At and Above Resonance

Abstract – The flying capacitor multilevel (FCML) converter has shown promise for high step-up/down conversion ratios due to its relatively low switch stress and small inductor volume. For higher level-count ($N \geq 3$) variations of this topology, there is limited research on resonant mode operation, despite its promise to yield considerable performance benefits. Using resonant mode operation, magnetic volume may be further reduced, transient response increased, and zero-voltage/zero-current switching (ZCS/ZVS) enabled at the cost of fixed conversion ratio operation. This work presents and analyzes a clocking scheme required to operate an N:1 FCML converter both at-resonance and above-resonance, while maintaining minimum current ripple for reduced losses. A complete derivation is presented, enabling the calculation of precise phase durations as a function of switching frequency. Moreover, a 5:1 FCML hardware prototype is demonstrated, verifying intended operation both at and above resonance, in addition to highlighting the achievable loss reduction with the proposed switching scheme.

I. Introduction

The flying capacitor multilevel (FCML) converter has gained popularity due to its high power density and high efficiency for both step-up and step-down conversion over a very wide conversion range [1], [2]. The FCML topology is often discussed as an attractive alternative to conventional buck or boost-type topologies due to its ability to regulate, greatly reduced inductance requirements, and decreased switch stress on the active devices—allowing the designer to take advantage of the better figures-of-merit for lower voltage switches [3]. However, the FCML converter can also be operated in a resonant mode as a fixed-ratio converter similar to other hybrid resonant switched-capacitor (SC) converters [4], [5]. As discussed in [6], [7], resonant operation of hybrid SC converters eliminates capacitor charge sharing losses, and allows for zero-current/voltage switching (ZCS/ZVS) to decrease switching losses. Furthermore, previous work has shown that operating hybrid SC converters above-resonance—at the fast-switching limit (FSL) [8]—can reduce the output impedance [9] and decrease sensitivity to component variation [10]. While operating above-resonance precludes ZCS, conduction and ac losses can be reduced due to the decreased rms currents compared to at-resonance operation. For high current applications, this is often a desirable trade-off.

Unlike many other hybrid SC converters, higher order ($N \geq 3$) resonant FCML converters require multi-resonant operation, with non-uniform resonant phase durations dependent on the level count, flying capacitance, and inductance. Previous work in [4], [9] proposed timings for a general 2 :1 resonant converter, as all hybrid SC converters collapse to this equivalent circuit for $N=2$; however, this analysis was not extended to higher level converters. Furthermore, [5] explored above-resonance operation of $N=3$ and $N=6$ FCML converters, but used a valley current control scheme to converge on optimal phase durations through active feedback. As such, no closed-form analytical solution to ideal phase timings has been published.

This work expands on prior analysis and provides an analytical solution to the optimal phase durations for a generic FCML operating at a fixed N :1 conversion for both at-resonance and above-resonance operation. The analysis presented here also provides a more general framework for analyzing other at- and above-resonance hybrid switched capacitor converters, though the FCML represents a more complex case due to the dependence of the phase durations on the relationship between the converter switching frequency and its natural resonant frequencies. Lastly, experimental results for a 5 :1 FCML converter are presented, validating the proposed analysis and demonstrating FCML performance at- and above-resonance.

II. Theory of Operation

Figure 1a shows a generic step-down N:1 FCML converter, where the input and output voltages are denoted as V_{HI} and V_{LO}, respectively. In this work, the parameter N refers to both the conversion ratio of the FCML converter as well as the number of complementary switch-pairs, $S_{NA/B}$. While the FCML converter can operate in resonance mode with fixed conversion ratios equal to or greater than $1/N$ (i.e., N:2, N:3, ...), this work will analyze the most extreme conversion ratio, N:1.

The gate timings of each switch pair, as shown in Fig. 2, are adjusted to ensure half-sine-wave (resonant) or a symmetric sine-wave segment (above resonance) inductor current in each phase, as illustrated in Fig. 3. To determine appropriate phase durations, charge flow analysis is performed [8]. While this analysis is suitable for any N:1 FCML, Fig. 1 depicts the circuit schematics for each phase of an example 5:1 step-down FCML converter where the charge q_H is defined as the product of the average current supplied by the high-side voltage, V_{HI}, and the switching period: $q_H = I_{HI} \cdot T_{\text{sw}}$. Phase 5 (Fig. 1f) is the only phase in which V_{HI} is connected, therefore, the charge supplied by V_{HI} in this phase must equal q_H.

Following the charge flow across phases, each flying capacitor is charged by q_H in one phase and discharged by q_H in one other phase, thereby maintaining charge balance across the capacitors in periodic steady-state. Because each flying capacitor is charged/discharged by the same charge quantity, equating all capacitances C_1 – C_{N-1} to an equivalent value, C_0, enforces equivalent voltage ripple magnitude on each of the flying capacitors. Finally, one q_H quantity is delivered to the low-side voltage, V_{LO} through inductor L during each of the five phases (N phases).

III. Calculating Phase Durations

To calculate ideal timing durations of each phase in periodic steady-state, the inductor current is assumed to start and end each phase at the same value, implying zero net volt-seconds across the inductor within each phase and minimized rms current ripple within a total period for reduced conduction and ac losses. Furthermore, for this analysis a high Q-factor is reasonably assumed for each phase configuration, leading to sinusoidal behavior with negligible damping.

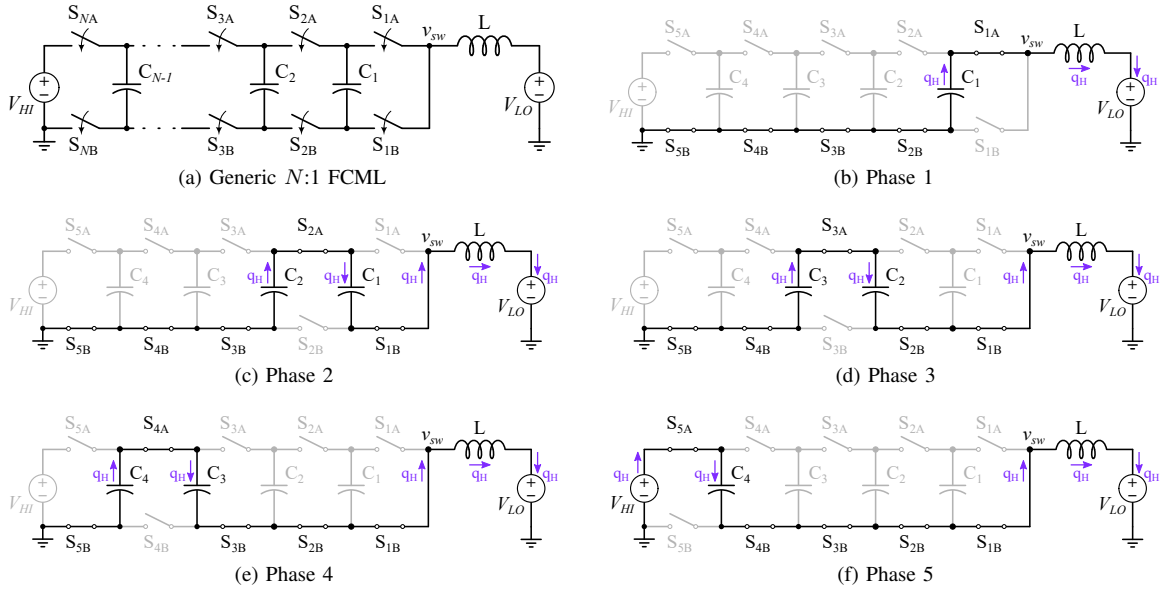

Fig. 1: Schematic for (a) a generic N:1 FCML converter, and (b)-(f) a 5:1 FCML converter, highlighting the charge flow during each phase, normalized with respect to high-side input charge quantity q_H.

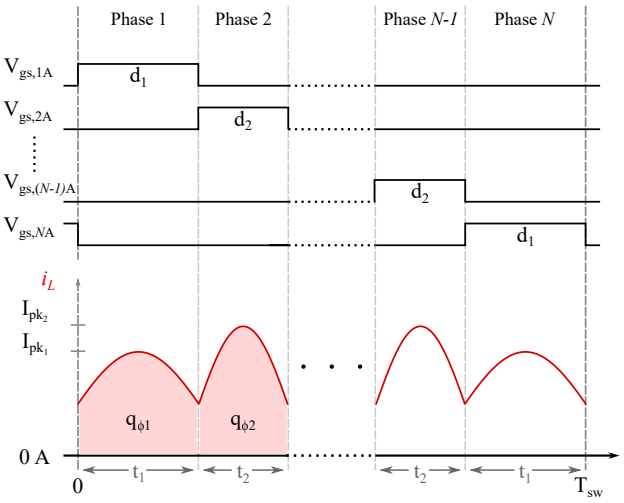

Fig. 2: Modulation scheme at- and above-resonance for N:1 FCML. The current i_L is shown for above-resonance.

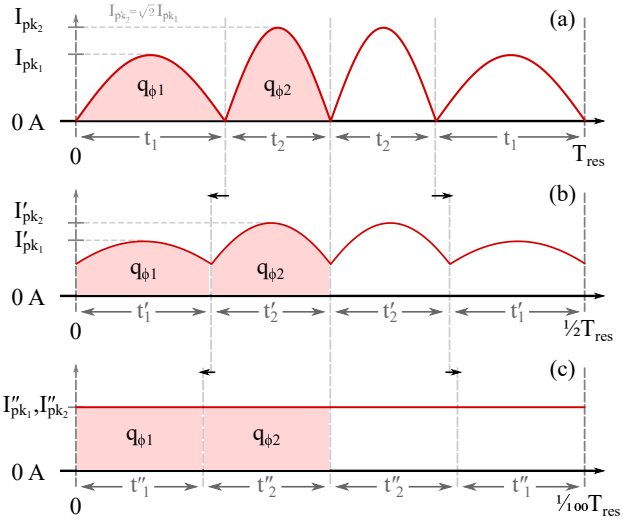

Fig. 3: Example 4:1 FCML inductor current waveforms at (a) $\Gamma = 1$, (b) $\Gamma = 0.5$, and (c) $\Gamma = 0.01$.

A. *At Resonance* ($\Gamma = 1$)

As shown in Fig. 1b and Fig.1f, only one flying capacitor with capacitance C_0 is connected in series with the inductor during phase 1 and phase N, allowing their resonant frequency, ω_{r1}, to be calculated using (1).

Similarly, all other phases $(2, 3, ..., N\text{-}1)$ are topologically equivalent, as they have two series-connected flying capacitors connected with the inductor. The resonant frequency in these phases can therefore be calculated using (2). The relationship between the two resonant frequencies can be found as shown in (3). Since equal charge q_H flows through the inductor during each phase ($q_H = I_{L,\text{avg}_i} \cdot t_{\phi_i}$), the relationship between the peak inductor currents, I_{pk_1} and I_{pk_2}, during each phase is determined by their resonant frequency ratio, yielding $\sqrt{2}\ I_{\text{pk}_1} = I_{\text{pk}_2}$. Example inductor current waveforms while operating at resonance can be seen in Fig. 3a.

$$\omega_{r1} = \frac{1}{\sqrt{LC_0}} \quad (1) \qquad \omega_{r2} = \frac{1}{\sqrt{L \cdot \left(\frac{1}{2}C_0\right)}} \quad (2) \qquad \sqrt{2}\ \omega_{r1} = \omega_{r2} \quad (3) \qquad \Gamma = \frac{f_{\text{sw,res}}}{f_{\text{sw}}} = \frac{T_{\text{sw}}}{T_{\text{sw,res}}} \quad (4)$$

B. *Above Resonance* ($\Gamma < 1$)

In considering operation of the FCML above resonance, we define the parameter Γ in (4), which relates the switching frequency of a full period f_{sw} to its value at full resonance $f_{\text{sw,res}}$. In the full resonant case Γ is unity, and as Γ decreases the switching frequency increases (i.e., above-resonance operation). To derive the proper duration of each phase for different Γ and N, a 'charge balance' and 'continuous current' constraint between phases is imposed on the inductor current.

1) 'Charge balance' constraint: The charge transferred, q_{ϕ_i}, during a phase ϕ_i is computed by integrating the instantaneous inductor current waveform $i_L(t)$—which is known generally for a resonant LC circuit—over the duration of each phase.

$$q_{\phi_2} = \int_{-\frac{t_2}{2}}^{\frac{t_2}{2}} I_{\text{pk}_2} \cos(\omega_{r2} t)\, dt = \frac{2I_{\text{pk}_2}}{\omega_{r2}} \sin\left(\omega_{r2}\frac{t_2}{2}\right) \quad (5) \qquad q_{\phi_1} = \int_{-\frac{t_1}{2}}^{\frac{t_1}{2}} I_{\text{pk}_1} \cos(\omega_{r1} t)\, dt = \frac{2I_{\text{pk}_1}}{\omega_{r1}} \sin\left(\omega_{r1}\frac{t_1}{2}\right) \quad (6)$$

The per-phase charges (5) and (6) are substituted into the FCML charge-balance relation (i.e., $q_{\phi_1} = q_{\phi_2} = ... = q_{\phi_N}$) to derive the first constraining equation in (7).

2) 'Continuous current' constraint: The second constraint enforces a continuous inductor current waveform, $i_L(t)$, between phases, as in (8). Moreover, the instantaneous current is assumed equal at all phase transitions (zero net volt-seconds).

$$q_{\phi_1} = q_{\phi_2} \quad \Rightarrow \quad \frac{I_{\text{pk}_1}}{I_{\text{pk}_2}} = \frac{\omega_{r1}}{\omega_{r2}} \cdot \frac{\sin\left(\frac{1}{2}\omega_{r2} t_2\right)}{\sin\left(\frac{1}{2}\omega_{r1} t_1\right)} \quad (7) \qquad I_{\text{pk}_1} \cos\left(\omega_{r1}\frac{t_1}{2}\right) = I_{\text{pk}_2} \cos\left(\omega_{r2}\frac{t_2}{2}\right) \quad \Rightarrow \quad \frac{I_{\text{pk}_1}}{I_{\text{pk}_2}} = \frac{\cos\left(\frac{1}{2}\omega_{r2} t_2\right)}{\cos\left(\frac{1}{2}\omega_{r1} t_1\right)} \quad (8)$$

3) Solving for phase durations: Substituting the 'charge balance' constraint (7) into the 'continuous current' constraint (8) yields an implicit equation (9) of t_1 and t_2, where the per-phase resonant frequencies ω_{r1} and ω_{r2} are known quantities for a specified L and C_0. A third constraining equation relates the sum of all phase durations to the switching period T_{sw} by (10).

$$\frac{\omega_{r1}}{\omega_{r2}} \cdot \frac{\sin\left(\frac{1}{2}\omega_{r2} t_2\right)}{\sin\left(\frac{1}{2}\omega_{r1} t_1\right)} = \frac{\cos\left(\frac{1}{2}\omega_{r2} t_2\right)}{\cos\left(\frac{1}{2}\omega_{r1} t_1\right)} \quad (9) \qquad T_{\text{sw}} = \sum_{i=1}^{N} t_{\phi_i} = 2\,t_1 + (N-2)\,t_2 \quad (10)$$

Since $\sqrt{2}\,\omega_{r1} = \omega_{r2}$ (3) for the resonant FCML, the implicit equation in (9) reduces no further and thus the phase durations cannot be determined analytically. Equation (9) can be rearranged to construct a minimization function $f(t_1, t_2)$ in (11) with constraint (10) to numerically solve for t_1 (and t_2).

$$f(t_1, t_2) = \left| \sin\left(\frac{1}{2}\omega_{r1}\,t_1 - \frac{1}{2}\omega_{r2}\,t_2\right) - \frac{\omega_{r1} - \omega_{r2}}{\omega_{r1} + \omega_{r2}} \cdot \sin\left(\frac{1}{2}\omega_{r1}\,t_1 + \frac{1}{2}\omega_{r2}\,t_2\right) \right| = 0 \quad (11)$$

From inspection of the numerical solution (an example $N = 5$ is shown in Fig. 4), an accurate closed-form expression of the relative phase durations t_1/T_{sw} and t_2/T_{sw} is approximated in (12) and (13) as a function of N and Γ only.

$$\frac{t_1}{T_{\text{sw}}} \approx \left(\frac{1}{N} - \frac{\sqrt{2}}{2\sqrt{2}+N-2}\right) \cdot \frac{\sin(\pi\Gamma)}{\pi\Gamma} + \frac{\sqrt{2}}{2\sqrt{2}+N-2} \quad (12) \qquad \frac{t_2}{T_{\text{sw}}} \approx \left(\frac{1}{N} - \frac{1}{2\sqrt{2}+N-2}\right) \cdot \frac{\sin(\pi\Gamma)}{\pi\Gamma} + \frac{1}{2\sqrt{2}+N-2} \quad (13)$$

These phase duration approximations can also be used to derive an approximation for the peak-to-average inductor current ratio in (14) which reduces to the precise value in (15) when at resonance ($\Gamma = 1$). For decreasing Γ and increasing N the peak inductor current decreases monotonically, as shown in Fig. 5, thus the expected conduction losses also decrease.

$$\frac{I_{\text{pk}}}{I_{out}} = \frac{I_{\text{pk}_2}}{I_{out}} \approx \frac{(2\sqrt{2}+N-2)\cdot\pi\Gamma}{2N \cdot \sin\left(\frac{\sqrt{2}-1}{N}\sin(\pi\Gamma) + \frac{\pi}{2}\Gamma\right)} \quad (14) \qquad \frac{I_{\text{pk}}}{I_{out}} = \left(\frac{2\sqrt{2}+N-2}{N}\right)\cdot\frac{\pi}{2} \quad \text{when } \Gamma = 1 \quad (15)$$

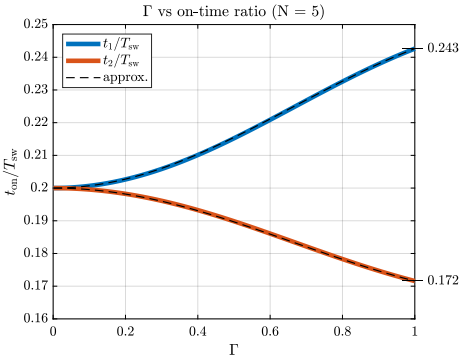

Fig. 4: Numerical solution of relative phase durations t_1/T_{sw} and t_2/T_{sw} for a 5:1 FCML across Γ. The closed-form approximations are superimposed with dashed lines.

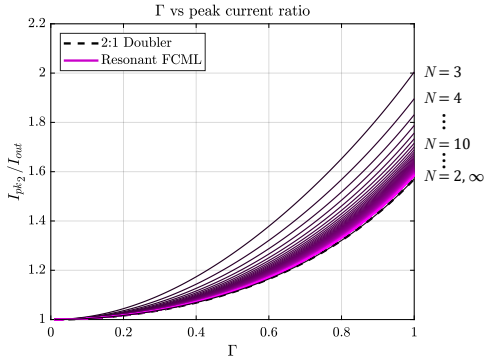

Fig. 5: Γ versus peak-to-average output current I_{out} for all N. Peak inductor current occurs during phases 2 to N-1, while two flying capacitors are connected in series.

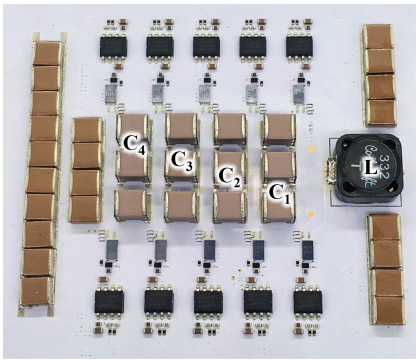

Fig. 6: Photograph of the constructed 5:1 FCML hardware prototype.

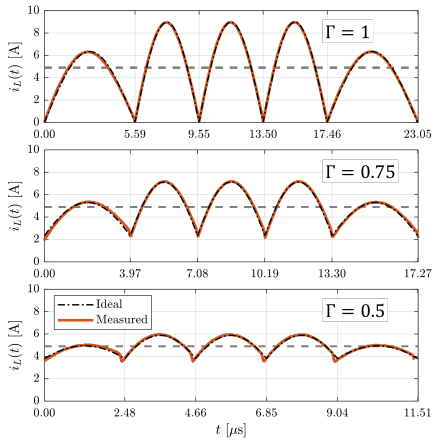

Fig. 7: Measured vs ideal inductor current waveforms for various Γ ($N = 5$, $I_{out} = 4.9$ A).

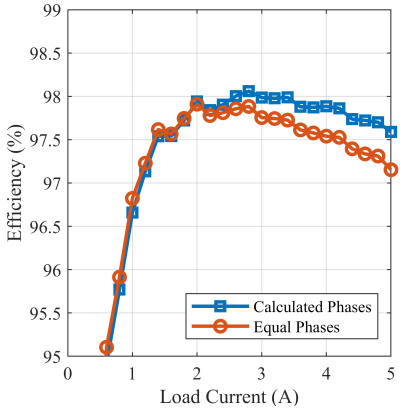

Fig. 8: Measured efficiency curves comparing FCML operation using the calculated phase durations, versus setting all phase durations equal in length. The latter sees up to a 19% increase in losses.

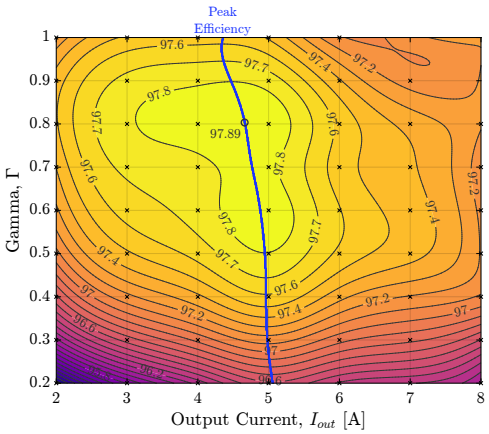

Fig. 9: Measured efficiency contour with swept I_{out} and Γ. Datapoints located on gridline intersections. $N = 5$, $V_{HI} = 200$ V, $L = 3.39$ μH, $C_0 = 0.93$ μF ($f_{\text{sw,res}} = 43.4$ kHz).

IV. Experimental Validation

Testing of the hardware prototype, shown in Fig. 6, validated that the approximate phase durations derived in (12) and (13) match experimental results both at- and above-resonance (i.e., $\Gamma \leq 1$) as shown in Fig. 7. Moreover, Fig. 8 illustrates up to a 15% decrease in converter losses when the derived optimal phase durations are used in place of equal phase intervals.

Efficiency, η, was also measured across a range of output current I_{out} and Γ; Fig. 9 illustrates an interpolated contour of these measured efficiencies. As Γ decreases below unity (i.e., f_{sw} increases), the efficiency is maximized in the region $0.5 < \Gamma < 0.9$. This hardware prototype demonstrates that above-resonance operation ($\Gamma < 1$) can result in an improved overall efficiency through the significant reduction of conduction losses despite losing ZCS and the increase of switching losses—a conclusion shared by [9]. Additionally, the point of peak efficiency appears invariant of load across the range of Γ.

V. Conclusion and Future Work

This work derives the closed-form solution for the phase durations required to operate an N:1 FCML at- and above-resonance, while simultaneously minimizing rms inductor current ripple for reduced overall converter loss. Furthermore, a general method for analyzing above-resonance behavior of hybrid switched-capacitor converters has been presented. The hardware prototype results for the 5:1 FCML converter match simulation closely and confirm the presented operation mode. The final paper will include further derivation details as well as additional hardware results.

References

[1] T. A. Meynard and H. Foch, "Multi-level conversion: high voltage choppers and voltage-source inverters," in *Power Electronics Specialists Conference, 1992. PESC '92 Record., 23rd Annual IEEE*, Jun 1992, pp. 397–403 vol.1.

[2] T. Modeer, N. Pallo, T. Foulkes, C. B. Barth, and R. C. N. Pilawa-Podgurski, "Design of a GaN-based interleaved nine-level flying capacitor multilevel inverter for electric aircraft applications," *IEEE Transactions on Power Electronics*, vol. 35, no. 11, pp. 12 153–12 165, 2020.

[3] J. T. Stauth, "Pathways to mm-scale dc-dc converters: Trends, opportunities, and limitations," in *2018 IEEE Custom Integrated Circuits Conference (CICC)*, 2018, pp. 1–8.

[4] K. Kesarwani and J. T. Stauth, "Resonant and multi-mode operation of flying capacitor multi-level dc-dc converters," in *2015 IEEE 16th Workshop on Control and Modeling for Power Electronics (COMPEL)*, 2015, pp. 1–8.

[5] C. Schaef, J. Rentmeister, and J. T. Stauth, "Multimode operation of resonant and hybrid switched-capacitor topologies," *IEEE Transactions on Power Electronics*, vol. 33, no. 12, pp. 10 512–10 523, Dec 2018.

[6] Y. Lei and R. C. N. Pilawa-Podgurski, "A general method for analyzing resonant and soft-charging operation of switched-capacitor converters," *IEEE Transactions on Power Electronics*, vol. 30, no. 10, pp. 5650–5664, 2015.

[7] S. R. Pasternak, M. H. Kiani, J. S. Rentmeister, and J. T. Stauth, "Modeling and performance limits of switched-capacitor dc–dc converters capable of resonant operation with a single inductor," *IEEE Journal of Emerging and Selected Topics in Power Electronics*, vol. 5, no. 4, pp. 1746–1760, 2017.

[8] M. Seeman and S. Sanders, "Analysis and optimization of switched-capacitor dc-dc converters," *Power Electronics, IEEE Transactions on*, vol. 23, no. 2, pp. 841–851, March 2008.

[9] J. S. Rentmeister and J. T. Stauth, "Multi-mode operation of resonant switched capacitor converters for optimized efficiency," in *2018 IEEE 19th Workshop on Control and Modeling for Power Electronics (COMPEL)*, 2018, pp. 1–7.

[10] Z. Ye, Y. Lei, and R. C. N. Pilawa-Podgurski, "The cascaded resonant converter: A hybrid switched-capacitor topology with high power density and efficiency," *IEEE Transactions on Power Electronics*, vol. 35, no. 5, pp. 4946–4958, 2020.